Inorganic Chemistry

Article

pubs.acs.org/IC

Antibacterial Action of 4,4′-Bipyrazolyl-Based Silver(I) Coordination Polymers Embedded in PE Disks

Aurel Tăbăcaru,[†] Claudio Pettinari,*[,†] Fabio Marchetti,[‡] Corrado di Nicola,[†] Konstantin V. Domasevitch,[§] Simona Galli,*[,∥] Norberto Masciocchi,[∥] Stefania Scuri,[⊥] Iolanda Grappasonni,[⊥] and Mario Cocchioni[⊥]

[†]Scuola di Scienze del Farmaco e dei Prodotti della Salute and [‡]Scuola di Scienze e Tecnologie, Divisione di Chimica, Università degli Studi di Camerino, Via S. Agostino 1, 62032 Camerino (MC), Italy

[§]National Taras Shevchenko University of Kyiv, Volodimirska Strasse 64, 01033 Kyiv, Ukraine

[∥]Dipartimento di Scienza e Alta Tecnologia, Università dell'Insubria, Via Valleggio 11, 22100 Como, Italy

[⊥]Centro Ricerche Scienze Igienistiche e Sanitarie Ambientali, Scuola di Scienze del Farmaco e dei Prodotti della Salute, Università degli Studi di Camerino, Via Madonna delle Carceri 9, 62032 Camerino (MC), Italy

Supporting Information

ABSTRACT: Coupling the rigid spacer 4,4′-bipyrazole (H_2BPZ), in its anionic or neutral form, to different silver(I) salts allowed isolation of the novel coordination polymers $[Ag_2(BPZ)]$ (**1**) and $[Ag(H_2BPZ)(X)]$ (X = NO_3, **2**; ClO_4, **3**; BF_4, **4**; PF_6, **5**; CH_3SO_3, **6**; CF_3SO_3, **7**), which were fully characterized by infrared and emission spectroscopies, thermal analysis, and X-ray powder diffraction. The crystal structure of **1** consists of 2-D layers containing 1-D chains of Ag(I) ions bridged by *exo*-tetradentate bipyrazolato moieties. The crystal structures of the $[Ag(H_2BPZ)(X)]$ species **2**−**7** feature 1-D chains of $[Ag(H_2BPZ)]$ stoichiometry, along which the metal centers are bridged by *exo*-bidentate bipyrazolyl spacers. Contacts among adjacent chains are mediated by the counterions through nonbonding interactions involving the Ag(I) ions and the pyrazolyl N−H groups. Thermogravimetric analyses disclosed the good thermal stability of these materials, decomposing in the range 200−300 °C. Under UV irradiation at room temperature, all the species showed a yellow-green emission centered in the range 520−522 nm. When embedded into polyethylene disks, **1**, **2**, and **4**−**7** demonstrated their activity as topical antibacterial agents against suspensions of *E. coli*, *P. aeruginosa*, and *S. aureus*: complete reduction of the three bacterial strains was achieved in 24 h, reduction of *S. aureus* reaching ca. 90% in only 2 h. Biocidal action was expressed also by contact susceptibility tests.

1. INTRODUCTION

In the past decade, massive attention has been focused on the design and characterization of silver(I)-based coordination polymers, which combine interesting structural topologies[1] with outstanding functional properties such as photoluminescence,[2] guest exchange or uptake,[3] permanent porosity,[4] conductivity,[5,2] supramolecular chirality,[6] magnetism,[7] and even antibacterial activity.[8]

Silver(I) coordination architectures are widely influenced by several factors, ranging from the coordination geometry of the metal center and the functionality of the ligands[9,1b] to the metal-to-ligand ratio,[10b,c] the nature of counteranions,[10] and the reaction conditions,[11] making this coinage metal a suitable candidate for the construction of fascinating structural motifs.[1]

Silver(I) coordination complexes are the subject of deep investigation for the photophysical properties they may display.[2] Lately, advanced applications have been individuated in this field: inter alia, they seem promising as light-emitting diodes owing to simultaneous occurrence of mesomorphism and luminescence even at room temperature,[12] as selective sensing films for small organic molecule vapors,[13] or as optical recording or sensing devices due to luminescence mecanochromism.[14]

Silver and silver(I)-based compounds are highly toxic to microorganisms, showing strong biocidal effects on as many as 12 species of bacteria, including *E. coli*.[15] Silver gained regulatory approval as a topical antimicrobial agent in the early 20th century. After progressive abandon due to introduction of antibiotics in the 1940s, it reacquired popularity, as witnessed, for instance, by studies carried out in the 1960s on silver(I) sulfadiazine,[16] which is currently commercialized as a topical antibacterial cream for burns and wounds. Currently, numerous are the applications in which

Received: June 1, 2012
Published: August 24, 2012

   dx.doi.org/10.1021/ic3011635 | *Inorg. Chem.* 2012, 51, 9775−9788

silver or silver(I) derivatives are involved as biocidal agents: from inclusion into antimicrobial ceramics[17] or catheters[18] to deposition as film coatings onto external fixation devices or bone matrices[19] or as nanoparticles onto textiles.[20]

Promising results on the antibacterial activity of silver(I)-based *coordination polymers*, when in suspension, were obtained already in 1997 by Nomiya and co-workers, who demonstrated that [Ag(im)] and [Ag(Him)$_2$](NO$_3$) (Him = 1,3-imidazole) possess a wide spectrum of antimicrobial and antifungal activities.[21a,b] Marked activities were also observed for [Ag(1,2,3-tz)],[21c] [Ag(1,2,4-tz)],[21c] [Ag(pz)],[21d] and [Ag(tetz)][21e] (Hpz = 1,2-pyrazole; 1,2,3-Htz = 1,2,3-triazole; 1,2,4-Htz = 1,2,4-triazole; Htetz =1,2,3,4-tetrazole). The performance of these materials was invariably more promising than those possessed by silver(I) complexes with *S*-based ligands.[21f−h] More recent results are exemplified by [Ag$_3$(3-phosphonobenzoate)],[8a] showing, in the form of powder, bactericidal action, [Ag(ethanediyl-bis(isonicotinate))(NO$_3$)],[8b] an effective antibacterial coating agent for dental implant applications, and the water-soluble species [Ag(L-acmet)] and [Ag$_2$(D-acmet)(L-acmet)] (acmet = acetylmethioninate), possessing wide-spectrum antimicrobial activity against Gram-negative bacteria and yeasts.[22]

The ditopic, rod-shaped ligand 4,4′-bipyrazole (H$_2$BPZ, Scheme 1) has been recently identified as a novel, versatile tecton in the construction of transition-metal-based coordination compounds, as demonstrated by the isolation and characterization of 1-D, 2-D, and 3-D coordination polymers of zinc(II), cobalt(II), cadmium(II), and copper(II),[23] as well as of nickel(II)-based polynuclear complexes.[24] The coordination modes of the corresponding dianion were first probed by Sun and co-workers, who reported that dipalladium(II,II) and diplatinum(II,II) clips can be bridged by BPZ^{2-} to give metallomacrocycles with interesting photophysical properties.[25]

Scheme 1. 4,4′-Bipyrazole (H$_2$BPZ)

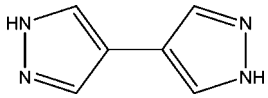

Our long-term experience with polyazolato-based coordination polymers[12,26] prompted us to direct our attention toward BPZ^{2-}, which has led to isolation of the porous and thermally robust coordination polymers [M(BPZ)]·Solv (M = Co, Ni, Zn, Cd).[27] Notably, no investigations have been carried out yet with the aim of coupling H$_2$BPZ, in its neutral or dianionic form, to silver(I) ions.

In this article, we demonstrate that reacting the rigid spacer H$_2$BPZ with silver(I) ions allows construction of the novel coordination polymers [Ag$_2$(BPZ)] (**1**) and [Ag(H$_2$BPZ)(X)] (X = NO$_3$, **2**; ClO$_4$, **3**; BF$_4$, **4**; PF$_6$, **5**; CH$_3$SO$_3$, **6**; CF$_3$SO$_3$, **7**), which couple, in the solid state, interesting antibacterial activity to room-temperature photoluminescence. The seven derivatives were isolated and fully characterized by means of infrared and emission spectroscopy, thermal analysis, and X-ray powder diffraction. Specific tests were carried out on **1**, **2**, and **4**−**7** embedded in polyethylene disks to probe their antimicrobial activity against suspensions of *E. coli*, *P. aeruginosa*, and *S. aureus*. Their topical biocidal action was further substantiated by contact susceptibility tests.

2. EXPERIMENTAL SECTION

2.1. Materials and Methods. All chemicals and reagents were purchased from Sigma Aldrich Co. and used as received without further purification. All solvents were distilled prior to use. 4,4′-Bipyrazole was synthesized following the method already reported in the literature.[23] IR spectra were recorded from 4000 to 650 cm^{-1} with a Perkin-Elmer Spectrum 100 instrument by total reflectance on a CdSe crystal. Elemental analyses (C, H, N, S) were performed with a Fisons Instruments 1108 CHNS-O elemental analyzer. Thermal-gravimetric analyses (TGA) were carried out in a N$_2$ stream with a Perkin-Elmer STA 6000 simultaneous thermal analyzer with a heating rate of 7 °C/min. Solid-state photoluminescence spectra were collected at room temperature with a Perkin-Elmer LS 45 luminescence spectrometer equipped with a pulsed Xe flash lamp.

2.2. Synthesis of [Ag$_2$(BPZ)] (1). H$_2$BPZ (0.067 g, 0.5 mmol) was dissolved in 30 mL of methanol. Separately, AgCl (0.143 g, 1 mmol) was dissolved in 30 mL of aqueous ammonia (30%) under gentle warming (45 °C). The resulting limpid solution was added to the first one with a dropping funnel. A white suspension immediately formed and was left under stirring at room temperature for 2 h. Then, the white precipitate was filtered off, washed twice with methanol, and dried under vacuum. Yield: 80%. **1** is insoluble in chlorinated solvents, alcohols, acetone, acetonitrile, DMSO, and water. IR (cm^{-1}): 3109(m) ν(C−H$_{aromatic}$), 1510(m) ν(C═C + C═N), 1375(s), 1272(s), 1160(s), 1040(vs), 917(s), 844(vs). Anal. Calcd for C$_6$H$_4$Ag$_2$N$_4$ (fw = 347.86 g/mol): C, 20.72; H, 1.16; N, 16.11. Found: C, 21.14; H, 1.18; N, 15.35. Compound **1** can be obtained also by reacting the H$_2$BPZ ligand with either AgCH$_3$COO or AgCF$_3$COO in ethanol/water (1:1 v/v) under gentle warming (45 °C) and stirring overnight.

2.3. Synthesis of [Ag(H$_2$BPZ)(NO$_3$)]·H$_2$O (2). H$_2$BPZ (0.067 g, 0.5 mmol) was dissolved in 30 mL of ethanol under gentle warming (45 °C). Then, AgNO$_3$ (0.169 g, 1 mmol) was added. The resulting white suspension was left under stirring at room temperature for 2 h, obtaining a white precipitate that was filtered off, washed twice with ethanol, and dried under vacuum. Yield: 75%. **2** is insoluble in chlorinated solvents, alcohols, acetone, acetonitrile, DMSO, and water. IR (cm^{-1}): 3444(w), 3352(w) ν(N−H), 3121(m), 3063(w) ν(C−H$_{aromatic}$), 1548(vw), 1501(w) ν(C═C + C═N), 1396(vs) ν_{asym}(NO$_3$), 1326(vs) ν_{sym}(NO$_3$), 1172(m), 1055(m), 967(m), 880(m), 772(m). Anal. Calcd for C$_6$H$_8$AgN$_5$O$_4$ (fw = 332.03 g/mol): C, 22.38; H, 2.50; N, 21.75. Found: C, 22.61; H, 2.33; N, 21.34.

2.4. Synthesis of [Ag(H$_2$BPZ)(ClO$_4$)] (3). H$_2$BPZ (0.067 g, 0.5 mmol) was dissolved in 30 mL of ethanol under gentle warming (45 °C). Then, AgClO$_4$ (0.207 g, 1 mmol) was added. The resulting white suspension was left under stirring at room temperature for 2 h, obtaining a white precipitate that was filtered off, washed twice with ethanol, and dried under vacuum. Yield: 85%. **3** is insoluble in chlorinated solvents, alcohols, acetone, acetonitrile, DMSO, and water. IR (cm^{-1}): 3286(m) ν(N−H), 3137(vw), 3118(vw) ν(C−H$_{aromatic}$), 1537(vw), 1483(w) ν(C═C + C═N), 1387(m), 1319(m), 1048(vs) ν(ClO$_4$), 963(s), 909(s), 869(s), 818(s), 697(s). Anal. Calcd for C$_6$H$_6$AgClN$_4$O$_4$ (fw = 341.46 g/mol): C, 21.11; H, 1.77; N, 16.41. Found: C, 21.18; H, 1.63; N, 16.09.

2.5. Synthesis of [Ag(H$_2$BPZ)(BF$_4$)] (4). H$_2$BPZ (0.067 g, 0.5 mmol) was dissolved in 30 mL of acetonitrile under gentle warming (45 °C). Then, (MeCN)$_4$AgBF$_4$ (0.358 g, 1 mmol) was added. The resulting white suspension was left under stirring at room temperature for 4 h, obtaining a white precipitate that was filtered off, washed twice with acetonitrile, and dried under vacuum. Yield: 80%. **4** is insoluble in chlorinated solvents, alcohols, acetone, acetonitrile, DMSO and water. IR (cm^{-1}): 3315(m) ν(N−H), 3149(vw), 3122(vw) ν(C−H$_{aromatic}$), 1538(vw), 1488(w) ν(C═C + C═N), 1388(m), 1319(m), 1169(m), 1049(vs), 1015(vs) ν(BF$_4$), 960(s), 909(s), 863(s), 817(s), 767(w), 684(s). Anal. Calcd for C$_6$H$_6$AgBF$_4$N$_4$ (fw = 328.81 g/mol): C, 21.92; H, 1.84; N, 17.04. Found: C, 22.18; H, 1.82; N, 16.80.

2.6. Synthesis of [Ag(H$_2$BPZ)(PF$_6$)] (5). H$_2$BPZ (0.067 g, 0.5 mmol) was dissolved in 30 mL of ethanol under gentle warming (45 °C). Then, AgPF$_6$ (0.253 g, 1 mmol) was added. The resulting white suspension was left under stirring at room temperature for 3 h,

dx.doi.org/10.1021/ic3011635 | Inorg. Chem. 2012, 51, 9775−9788

Table 1. Crystallochemically Relevant Data for Species 1−7 and 2a

	1	2	2a	3	4	5	6	7
empirical formula	$C_6H_4Ag_2N_4$	$C_6H_8AgN_5O_4$	$C_6H_6AgN_5O_3$	$C_6H_6AgClN_4O_4$	$C_6H_6AgBF_4N_4$	$C_6H_6AgF_6N_4P$	$C_7H_9AgN_4O_3S$	$C_7H_6AgF_3N_4O_3S$
fw, g mol^{-1}	347.9	322.0	304.0	341.4	328.8	387.0	337.1	391.1
T, °C	25	25	200	25	25	25	25	25
cryst syst	monoclinic	triclinic	triclinic	triclinic	monoclinic	triclinic	orthorhombic	monoclinic
SPGR, Z	$P2_1/c$, 2	P-1, 2	P-1, 1	P-1, 2	Pc, 2	P-1, 2	$Pnna$, 4	$P2_1$, 2
a, Å	9.1210(7)	5.5420(2)	5.2708(3)	6.8199(1)	5.2798(1)	5.2884(2)	6.7805(2)	9.9963(3)
b, Å	6.1455(5)	8.4098(3)	6.7685(4)	7.7967(2)	7.8059(2)	9.7027(4)	15.6464(5)	6.8000(2)
c, Å	6.6294(5)	11.3237(4)	7.2141(3)	10.0136(2)	13.1634(4)	11.6557(5)	10.0392(3)	8.6352(3)
α, deg	90	74.085(2)	94.818(6)	97.123(2)	90	101.794(2)	90	90
β, deg	95.24(9)	83.081(3)	82.403(5)	104.341(2)	112.865(2)	102.020(3)	90	92.035(2)
γ, deg	90	85.382(3)	111.993(3)	80.502(2)	90	105.059(2)	90	90
V, Å^3	370.05(5)	503.21(3)	236.37(2)	506.85(2)	499.89(2)	543.30(4)	1065.06(6)	586.61(3)
ρ, g/cm^3	1.13	0.77	0.77	0.81	0.79	0.86	0.76	0.80
μ(Cu Kα), cm^{-1}	419.1	162.1	171.2	184.9	165.7	170.3	170.4	159.7
F(000)	324	316	140	332	314	372	664	760
R_p, R_{wp}	0.034, 0.049	0.045, 0.059	0.040, 0.054	0.057, 0.077	0.054, 0.073	0.048, 0.064	0.076, 0.106	0.070, 0.102
R_{Bragg}	0.026	0.026	0.017	0.032	0.039	0.035	0.059	0.059

obtaining a white precipitate that was filtered off, washed twice with ethanol, and dried under vacuum. Yield: 90%. **5** is insoluble in chlorinated solvents, alcohols, acetone, acetonitrile, DMSO, and water. IR (cm^{-1}): 3404(m) ν(N−H), 3146(vw) ν(C−H$_{aromatic}$), 1538(vw), 1480(w) ν(C═C + C═N), 1390(m), 1145(m), 1054(m), 809(vs) ν(PF_6), 670(s). Anal. Calcd for $C_6H_6AgF_6N_4P$ (fw = 386.97 g/mol): C, 18.62; H, 1.56; N, 14.48. Found: C, 19.21; H, 1.31; N, 14.05.

2.7. Synthesis of [Ag(H$_2$BPZ)(CH$_3$SO$_3$)] (6). H_2BPZ (0.067 g, 0.5 mmol) was dissolved in 30 mL of ethanol under gentle warming (45 °C). Then, $AgCH_3SO_3$ (0.203 g, 1 mmol) was added. The resulting white suspension was left under stirring at room temperature for 4 h, obtaining a white precipitate that was filtered off, washed twice with ethanol, and dried under vacuum. Yield: 75%. **6** is insoluble in chlorinated solvents, alcohols, acetone, acetonitrile, DMSO, and water. IR (cm^{-1}): 3182(m), 3159(m) ν(N−H), 3128(m), 3061(w) ν(C−H$_{aromatic}$), 2930(w) (CH_3), 1547(w), 1501(w) ν(C═C + C═N), 1382(w), 1220(vs), 1175(s), 1144(vs), 1054(m), 1030(vs) ν-(CH_3SO_3), 969(m), 851(s), 776(vs). Anal. Calcd for $C_7H_9AgN_4O_3S$ (fw = 337.11 g/mol): C, 24.94; H, 2.69; N, 16.62; S, 9.51. Found: C, 25.06; H, 2.55; N, 16.35; S, 9.76.

2.8. Synthesis of [Ag(H$_2$BPZ)(CF$_3$SO$_3$)] (7). H_2BPZ (0.067 g, 0.5 mmol) was dissolved in 30 mL of ethanol under gentle warming (45 °C). Then, $AgCF_3SO_3$ (0.257 g, 1 mmol) was added. The resulting white suspension was left under stirring at room temperature for 4 h, obtaining a white precipitate that was filtered off, washed twice with ethanol, and dried under vacuum. Yield: 70%. **7** is insoluble in chlorinated solvents, alcohols, acetone, acetonitrile, DMSO, and water. IR (cm^{-1}): 3223(m), 3172(m) ν(N−H), 3143(m), 3058(w) ν(C−H$_{aromatic}$), 1543(vw), 1497(w) ν(C═C + C═N), 1385(m), 1280(s), 1234(vs), 1221(vs), 1163(vs), 1145(vs), 1054(m), 1026(vs) ν-(CF_3SO_3), 966(m), 911(m), 863(m), 760(m). Anal. Calcd for $C_7H_6AgF_3N_4O_3S$ (fw = 391.08 g/mol): C, 21.50; H, 1.55; N, 14.33; S, 8.20. Found: C, 21.77; H, 1.27; N, 13.83; S, 8.41.

2.9. X-ray Powder Diffraction Structural Analysis. Polycrystalline samples of compounds **1**−**7**, not containing single crystals of suitable quality, were gently ground in an agate mortar. Then, they were deposited in the hollow of an aluminum sample holder equipped with a zero-background plate. The anhydrous species [Ag(H_2BPZ)-(NO_3)] (**2a**) was generated in situ depositing a powdered sample of the parent species **2** on an aluminum sample holder, heating it up to 200 °C by means of a custom-made sample heater (assembled by Officina Elettrotecnica di Tenno, Ponte Arche, Italy), and maintaining it at 200 °C during all data collection (**2a** transforms back into **2** if left a few minutes in air, XRPD evidence). For all species, diffraction data were collected by means of overnight scans in the 2θ range of 5−105°, with steps of 0.02°, on a Bruker AXS D8 Advance diffractometer, equipped with Ni-filtered Cu Kα radiation (λ = 1.5418 Å), with a Lynxeye linear position-sensitive detector, and with the following optics: primary beam Soller slits (2.3°), fixed divergence slit (0.5°), receiving slit (8 mm). The nominal resolution for the present setup is 0.08° of 2θ (fwhm of the α_1 component) for the LaB_6 peak at about 2θ = 21.3°. The generator was set at 40 kV and 40 mA. Standard peak search, followed by indexing through the single-value decomposition approach[28] implemented in TOPAS-R,[29] allowed detection of the approximate unit cell parameters of all species. Space groups were assigned on the basis of the systematic absences. Prior to structure solution, unit cells and space groups were controlled by means of structureless Le Bail refinements. Structure solutions were performed by the simulated annealing technique, implemented in TOPAS, employing a rigid, idealized model for the crystallographically independent portions of the ligand and the anions.[30] Final refinements were carried out by the Rietveld method, maintaining the rigid bodies introduced at the solution stage. The background was modeled by a Chebyshev polynomial function. One, isotropic thermal parameter was assigned to the metal atoms (B_M) and refined; lighter atoms were given a B_{iso} = B_M + 2.0 Å^2 thermal parameter. Preferred orientation corrections were introduced (in the March−Dollase formulation) along the [0 −1 1] and [1 0 0] directions for species **5** and **7**, respectively.

A summary of crystal data and data collection parameters is presented in Table 1. Final Rietveld refinement plots are shown in Figures S1−S3, Supporting Information. Fractional atomic coordinates are supplied in the Supporting Information as CIF files. X-ray crystallographic data in CIF format have been deposited at the Cambridge Crystallographic Data Center as supplementary publication nos. 880643−880650. Copies of the data can be obtained free of charge on application to the Director, CCDC, 12 Union Road, Cambridge, CB2 1EZ, U.K. (fax +44-1223-335033; e-mail deposit@ccdc.cam.ac.uk or http://www.ccdc.cam.ac.uk).

2.10. Variable-Temperature X-ray Powder Diffraction. Variable-temperature X-ray powder diffraction (TXRPD) experiments were performed on the as-synthesized species **2** to highlight its "structural" response to thermally induced solvent loss. Experiments were carried out in air using a custom-made sample heater, assembled by Officina Elettrotecnica di Tenno, Ponte Arche, Italy. Powdered polycrystalline samples of **2** were ground in an agate mortar and deposited in the hollow of an aluminum sample holder. Diffractograms were acquired in a significant low-angle 2θ range, heating in situ, with steps of 20 °C, from 30 °C up to loss of crystallinity. When comparing the TG and TXRPD results, the reader must be aware that the

dx.doi.org/10.1021/ic3011635 | Inorg. Chem. 2012, 51, 9775−9788

thermocouple of the TXRPD setup is *not* in direct contact with the sample, this determining a slight difference in the temperature at which the same event is detected by the two techniques. TG temperatures have to be considered as more reliable.

2.11. Silver(I) Coordination Polymers Embedding in Polyethylene Disks: Polymer Matrix Procedure. Polyethylene (PE) disks with embedded the species **1**, **2**, and **4**−**7** were prepared in the following manner: the coordination polymer, in the form of powder, was mixed in a glass capsule with PE granular powder (1.00 g) in a 1:50 weight ratio. The capsule was heated up to the melting point of PE (98 °C), while its content was stirred to give a homogeneous dispersion. The dispersion was then left to cool at room temperature; after solidification, the loaded polymer matrix was removed from the capsule and placed in contact with a hot quartz surface (130 °C): within a few minutes, the matrix melted and distributed homogeneously onto the quartz surface to give a thin liquid layer. After reduction of the quartz surface temperature down to 80 °C, the polymeric matrix layer turned into a soft solid film, suitable to be cut into small disks of 6 mm diameter and of thickness in the range 0.8−1.0 mm (see Figure 1). An unloaded PE disk was prepared and used as negative control. A PE disk with embedded silver nitrate was also prepared and used as positive control.

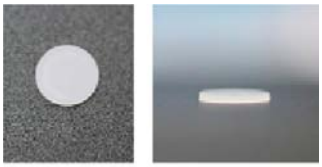

Figure 1. Example of a PE disk of 6 mm diameter and 0.8−1.0 mm thickness, prepared by the polymer matrix procedure: frontal (a) and lateral view (b).

To certify the embedding, scanning electron microscope (SEM) images of the disks were acquired, both for the side contacted with the hot quartz surface (magnifying at 500×, 1500×, and 10 000×) and for the back side (magnifying at 500× and 1500×). Specimens were mounted on a stub, coated with carbon, and then analyzed with a Stereoscan 360 SEM (Cambridge) equipped with an energy-dispersive X-ray detection system (AMPTEK XR-100CR). Images were acquired for a period of 100 s using secondary or backscattered electrons modes with an accelerating voltage of 15 kV. Brighter regions detected by SEM on the front side of the disks were analyzed by X-ray fluorescence (XRF) to prove the presence of silver. SEM images and XRF are reported in the Supporting Information.

To quantify the amount of Ag(I) released, PE disks loaded with the coordination polymers and containing nearly the same amount of silver were left in distilled water, at room temperature, under stirring. The content in Ag(I) of the suspending liquid was checked after 24, 48, and 72 h by means of an ICP-AES Jobin Yvon mod JY 24R spectrometer.

2.12. Microbiological Studies. The antibacterial activity of species **1**, **2**, and **4**−**7** embedded into PE disks was tested against the two Gram-negative bacteria *E. coli* ATCC 25922 (PBI International) and *P. aeruginosa* ATCC 27853 (OXOID-remel) and the Gram-positive bacteria *S. aureus* ATCC 25923 (PBI International). Bacteria were grown aerobically at 37 °C for 18 h using Tryptone Soya Broth (OXOID) as the growth medium.

Bacterial cultures in the range of 1−3 × 10^6 CFU/mL were added to sterilized test tubes containing 4 mL of autoclaved physiological solution. For sterilization of the tubes, an Alfa-10-plus autoclave (PBI International) was used, operating at 121 °C for 15 min. A 40 mg amount of loaded PE disk, previously reduced to granules, was added to the test tubes containing bacterial suspensions. All tubes were kept on an IKA KS 130 BASIC agitator for 24 h at slow speed. To study the growth inhibitory effect of the silver(I) derivatives on the bacterial cultures, 100 μL of supernatant fraction were withdrawn from the tubes at time intervals of 2, 4, 6, 24, 48, 72, and 96 h. To obtain the bacterial colony count, the supernatant fraction was diluted and included uniformly into Petri dishes containing Plate Count Agar (OXOID). Adopting the same procedure, an unloaded PE disk was used as negative control, while a PE disk embedded with $AgNO_3$ was used as positive control. In addition, we conducted a preliminary test to evaluate the bactericidal effect of the loaded PE disks by contact. To this aim, 0.5 mL of the bacterial aqueous suspension (*E. coli* 10^6 CFU/ml) was streaked over a plate containing m-Faecal Coliform Agar (m-FC), selective medium for faecal coliforms isolation and enumeration (OXOID S.p.A), and were spread uniformly. Embedded PE disks and the blank disk were gently placed over contaminated m-FC medium in Petri dishes. Petri dishes were incubated overnight at 44 °C for 24 h. After incubation, growth inhibition was evaluated by visual inspection, observing the dish, inverted, on a light table (Precision Illuminator, model B95, Northern Light).

3. RESULTS AND DISCUSSION

3.1. Synthesis, Stability, and Infrared Spectroscopy. The homoleptic derivative $[Ag_2(BPZ)]$ (**1**) can be isolated by employing silver chloride as the source of silver(I) ions in the presence of ammonia: the resulting cationic complex $[Ag(NH_3)_2]^+$ reacts at room temperature with H_2BPZ dissolved in methanol, yielding **1** in the form of a white polycrystalline powder. A similar synthetic strategy, involving ammonia solutions of silver(I) salts, was originally applied to recover the so-called Buchner's "silber salz" $[Ag(pz)]$[31] and, more recently, for the two supramolecular isomers $[Ag_2(Me_4BPZ)]\cdot Solv$ (Me_4BPZ = 3,3′,5,5′-tetramethyl-4,4′-bipyrazolyl).[4]

Independent on the silver(I):ligand molar ratio, when other silver salts are essayed in alcohols or acetonitrile at room temperature, coordination compounds having general formula $[Ag(H_2BPZ)(X)]$ are isolated (X = NO_3, **2**; ClO_4, **3**; BF_4, **4**; PF_6, **5**; CH_3SO_3, **6**; CF_3SO_3, **7**), as already observed with $[Ag(Me_4BPZ)(NO_3)]\cdot CH_3OH$,[32] $[Ag(Me_4BPZ)(ClO_4)]$,[33] and $[Ag(Me_4BPZ)(CF_3SO_3)]$.[33]

All Ag(I) derivatives precipitate in the form of white polycrystalline powders, air stable and insensitive to moisture. They are insoluble in water and in the most common organic solvents, this occurrence suggesting their polymeric nature. Their elemental analyses and IR spectra are unchanged after several weeks at room temperature and also after moderate thermal treatment (up to 120 °C). As detailed in the section devoted to their thermal behavior, they also possess a good thermal robustness: apart from dehydration of **2**, thermal treatment under nitrogen does not provoke thermal events before decomposition, which is observed at temperatures in the range 200−300 °C. Of greater importance in view of the investigations carried out upon their antibacterial activity (see below), all Ag(I) coordination polymers are recovered intact from water and physiological solutions.

Their infrared spectra are consistent with the proposed formulations (Figures S4−S6, Supporting Information). The IR spectrum of **1** displays a medium-intensity absorption band at 1510 cm^{-1}, which can be attributed to the so-called breathing of the pyrazolyl rings. The absence of IR bands due to N−H stretching clearly indicates that in **1** the ligand is deprotonated. On the contrary, in the case of species **2**−**7**, the medium-intensity absorption bands centered in the range 3200−3450 cm^{-1} can be attributed to the stretching vibrations of the N−H groups, as expected for the bipyrazolyl ligand in its neutral form. In **2**, the broadness of this band (extending in the range 2700−3400 cm^{-1}) suggests that the N−H groups are involved

dx.doi.org/10.1021/ic3011635 | *Inorg. Chem.* 2012, 51, 9775−9788

in strong hydrogen-bond interactions (see the description of the crystal structure and the caption to Figure 4). Again in **2**, the weak bands at 3444 and 1655 cm^{-1} can be ascribed to the stretching and bending vibrations of the clathrated water molecules. A detailed analysis of the IR spectra of **2**−**7** may also give hints about the interactions involving the anions. Thus, in the spectrum of **2**, the bands at 1396 and 1326 cm^{-1} and the very weak one in the overtone region (1700−1800 cm^{-1}) can be ascribed to the nitrate group (asymmetric and symmetric stretching modes and combination of symmetric stretching and in-plane bending, respectively). In particular, as originally proposed by Lever, the presence of a single band in the overtone region is indicative of a noncoordinated nitrate anion.[34] The IR spectrum of **3** shows two absorption bands characteristic of the perchlorate group: a strong and broad one in the region 1110−1050 cm^{-1} and a medium and broad one at 697 cm^{-1}.[35] In the IR spectrum of **4**, the fine splitting of the strong broad band in the region 1000−1100 cm^{-1} along with the presence of a weak band at 767 cm^{-1} and a medium broad one at 684 cm^{-1} indicate BF_4^- coordination at the silver(I) ions.[35] Analogously, the IR spectrum of **5**, displaying a strong broad band at 809 cm^{-1} and a medium broad one at 670 cm^{-1}, is in accordance with the existence of interactions between the PF_6^- anion and the silver(I) centers.[34] IR spectra of **6** and **7** show a number of strong absorptions in the 1180−1100 cm^{-1} region, due to the asymmetric and symmetric vibrations of the SO_3^- groups and vibration of the S−O moiety.[36]

3.2. Thermal Behavior. The thermal behavior of compounds **1**−**7** was investigated, under nitrogen, by thermogravimetric analyses. The resulting TGA traces are collectively depicted in Figure S7, Supporting Information. Only for **2**, which is the only species showing a thermal event before decomposition, TGA was complemented with in situ variable-temperature X-ray powder diffraction experiments (TXRPD), carried out in air.

*3.2.1. Thermal Behavior of [Ag_2(BPZ)], **1**.* Compound **1** is stable up to ca. 200 °C, the temperature at which progressive decomposition starts. At the end of the heating process, a black residue, possibly a mixture of metallic silver and some carbonaceous species, is recovered. The decomposition temperature of **1** is lower than that of the two [Ag_2(Me_4bpz)] supramolecular isomers (300 and 500 °C),[4b,c] featuring 3-D networks, but also than that of the simpler [Ag(pz)] analogue (270 °C), possessing a lower dimensionality architecture.[40] This possibly suggests that the thermal robustness of the material depends on the stability of the ligand more than on that of the overall framework.[37]

*3.2.2. Thermal Behavior of [Ag(H_2BPZ)(X)], **2**−**7**.* As for the [Ag(H_2BPZ)(X)] derivatives, only the hydrated species **2** undergoes a thermal event before decomposition. Indeed, its thermogravimetric trace shows a weight loss of ca. 5% in the temperature range 30−80 °C, which can be attributed to loss of one water molecule per formula unit (theoretical loss 5.6%). The anhydrous phase is stable up to ca. 250 °C, the temperature at which progressive decomposition begins. As shown by its thermodiffractogram (Figure 2), around 70 °C dehydration of **2** brings about a phase transformation to a nonisomorphous, anhydrous counterpart (**2a**). Further heating of **2a** modifies its unit cell parameters up to 200 °C, the temperature at which an asymptote is reached.

Of the remaining [Ag(H_2BPZ)(X)] compounds, **4** and **5** possess a moderate thermal robustness. **4** is stable up to ca. 275 °C. Then, a two-step decomposition process is observed: the first step takes place in the range 275−350 °C, and it is accompanied by a weight loss of ca. 20%, which can be interpreted as evolution of one BF_3 molecule per formula unit (theoretical loss 20.6%); the subsequent decomposition step spans the range 350−450 °C. Species **5** shows the lowest thermal stability, its decomposition beginning at about 250 °C. Finally, **3**, **6**, and **7** possess the highest thermal stability of the whole series: they survive up to ca. 300 (**6**) or 370 °C (**3** and **7**), the temperature at which they start to decompose (a strong exothermic effect is observed in the case of **3**, due to the well-known explosive character of the perchlorate anions). No comparison is possible with the family [Ag(Me_4BPZ)(X)] (X = NO_3,[32] ClO_4, or CF_3SO_3[33]), the thermal behavior of which was not investigated.

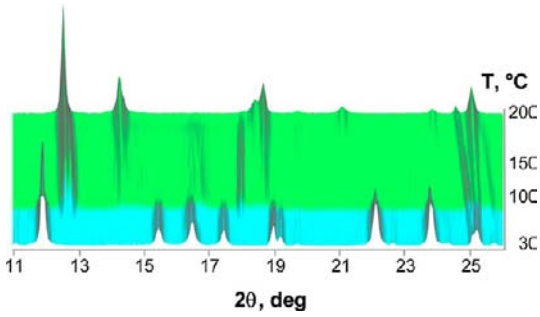

Figure 2. Plot of the X-ray powder diffraction patterns measured as a function of temperature, in the range 30−200 °C, to highlight the phase transformation accompanying dehydration of **2** (cyan portion) toward **2a** (light green portion).

3.3. Crystal Structures Analysis. All crystal and molecular structures discussed hereafter have been retrieved from state-of-the-art structural powder diffraction methods. Crystallochemically relevant details are gathered in Table 1, while the main geometrical parameters are provided throughout the text and in the pertinent figure captions.

*3.3.1. Crystal Structure of [Ag_2(BPZ)], **1**.* Compound **1** crystallizes in the monoclinic space group $P2_1/c$. The metal centers are bridged by the pyrazolato moieties of the BPZ^{2-} ligands along 1-D zig-zagged chains, which run parallel to the crystallographic axis *b* and whose shape is dictated by the 2_1 screw axis aligned with *b* (Figure 3a). Through the chains, argentophilic interactions can be envisaged (Ag···Ag 3.232(3) Å, Ag···Ag···Ag 143.9(3)°). Within the (1 0 −2) plane, the chains are reciprocally connected (and the metal ions are kept 9.426(4) Å apart) by the BPZ^{2-} moieties, creating 2-D corrugated layers (Figure 3b) stacked along the crystallographic axis *c* with a pace equal to *c*/2 (Figure 3c). Overall, the metal centers show a diagonal bent geometry, while the ligands show an *exo*-tetradentate coordination mode.

Notably, the crystal structure of **1** does not feature the Ag_3(ligand)$_3$ trigonal subunits which were devised in the trimeric phases [Ag_3(pz)$_3$][40] and [Au_3(pz)$_3$],[38] in other substituted pyrazolates of the coinage metals,[38,39] and even when bipyrazolates are involved, as exemplified by the 3-D coordination networks of both [Ag_2(Me_4bpz)] phases, where the trigonal units behave as three-connected nodes, linked by the C−C single bonds.[4b,c] On the other hand, the structural topology of **1** partially resembles that of the coordination polymers [M(pz)] (M = Cu, Ag; H_2pz = 1,2-pyrazole):[40] also in that case, 1-D zig-zagged chains were individuated (the two Cu(II) polymorphs differed in the interchain Cu···Cu contacts); obviously, the higher supramolecular dimensionality

dx.doi.org/10.1021/ic3011635 | Inorg. Chem. 2012, 51, 9775−9788

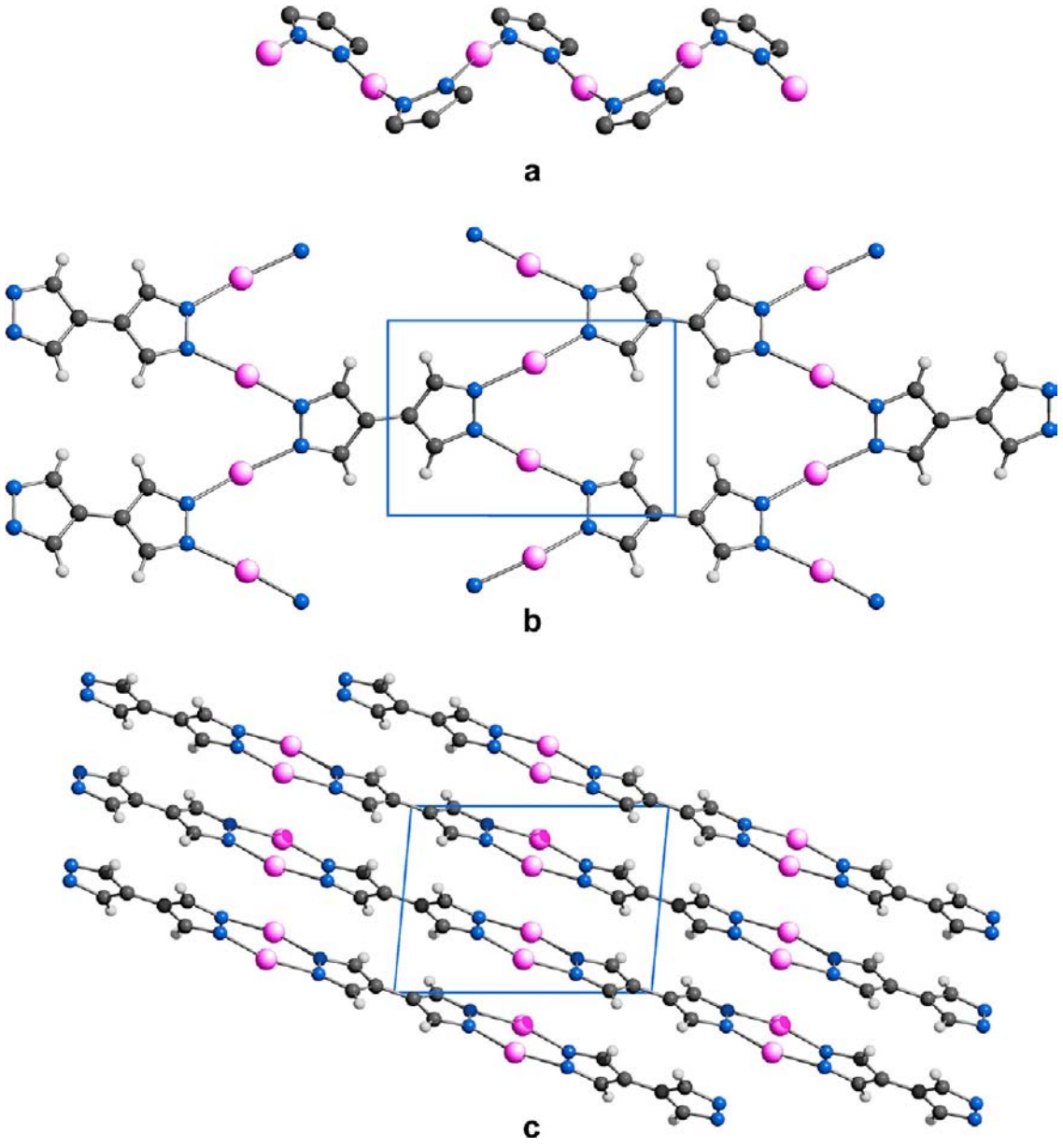

Figure 3. Representation of the crystal structure of species **1**: (a) 1-D zig-zagged chain running along *c*. (b) 2-D layer, viewed along *c* (horizontal axis, *a*; vertical axis, *b*). (c) Stacking of the 2-D layers, viewed along *b* (horizontal axis, *a*; vertical axis, *c*). Carbon, gray; hydrogen, light gray; nitrogen, blue; silver, fuchsia. Significant bond distances (Angstroms) and angles (degrees): Ag–N 2.107(4), 2.126(8); intrachain Ag···Ag, 3.232(3); BPZ-bridged Ag···Ag, 9.426(4); N–Ag–N, 167.1(3); intrachain Ag···Ag···Ag, 143.9(3).

promoted by the tetradentate BPZ^{2-} spacer could not be attained with the bidentate pz^{-} moiety.

*3.3.2. Crystal Structures of [Ag(H$_2$BPZ)(X)], **2**–**7** and **2a**.* All crystal structures of the $[Ag(H_2BPZ)(X)]$ species feature stacks of 1-D chains of $[Ag(H_2BPZ)]$ stoichiometry, along which the metal centers are bridged through the pyrazolyl moieties of *N,N′-exo*-bidentate spacers. The contacts among the chains of adjacent stacks are mediated by the counterions through long interactions (i) with the Ag(I) ions, formally resulting in a T-shaped stereochemistry at the metal ions, and (ii) with the pyrazolyl N–H groups. In the following, for the sake of completeness, further details are given for each crystal structure.

Compounds **2**, **3**, and **5** crystallize in the triclinic space group *P*-1. As anticipated above and depicted in Figures 4–6, all structures feature 1-D chains running approximately parallel to the [1 0 −1], [0 0 1], or [1 −1 −2] directions and stacking in columns approximately along the [1 0 3], [1 0 0], or [1 1 1] ones in **2**, **3**, or **5**, respectively. Along the chains, collinear Ag(I) ions are bridged by *exo*-bidentate H_2BPZ linkers and kept at a distance of about 10 Å. In all three structures the counterions are located in the space left between the stacks of chains but interact with the surroundings in different ways. In the case of **2**, the T-shaped stereochemistry of each metal center is granted by a long Ag···O interaction involving one oxygen atom of the counterion (Figure 4).

The latter is further involved in a hydrogen-bond interaction with a nearby N–H moiety belonging to the same chain- inter alia, this is the only hydrogen bond in the crystal structures of the $[Ag(H_2BPZ)(X)]$ species whose strength is high enough to leave a trace in the IR spectrum of the material (see above). This interaction is part of an intricate net of hydrogen bonds,

dx.doi.org/10.1021/ic3011635 | *Inorg. Chem.* 2012, 51, 9775–9788

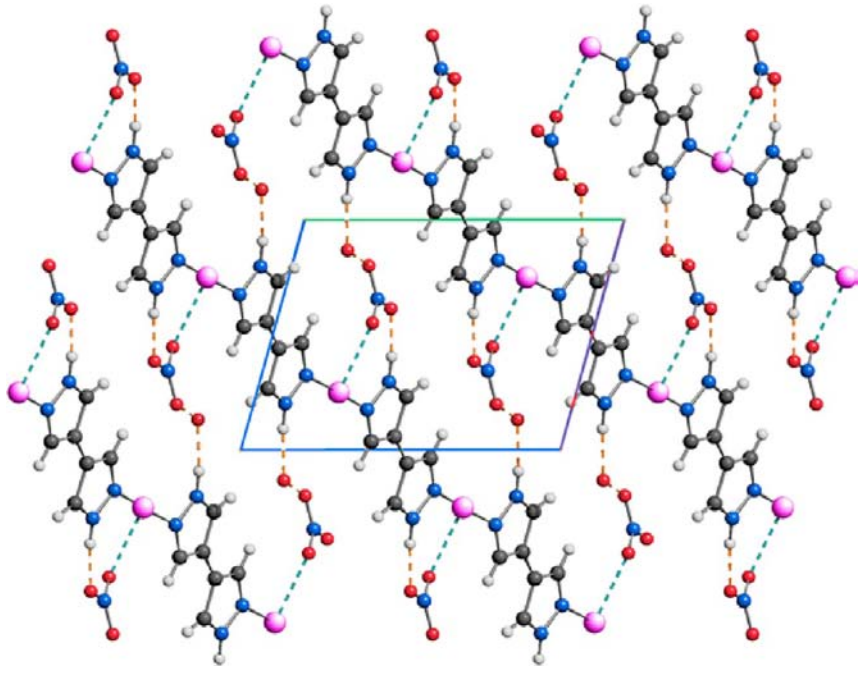

Figure 4. Representation of the crystal structure of species **2** viewed along *a*. Horizontal axis, *b*; vertical axis, *c*. Carbon, gray; hydrogen, light gray; nitrogen, blue; oxygen, red; silver, fuchsia. Long Ag···O interactions and hydrogen bonds are depicted with cyano and orange fragmented lines, respectively. For clarity, only some of the $O_{nitrate}$···O_{water} hydrogen-bond interactions have been depicted. Significant bond distances (Angstroms) and angles (degrees): Ag–N 2.119(8), 2.136(6); Ag···O 2.78(2); O···N–H 2.72(2), 2.81(2); $O_{nitrate}$···O_{water} 2.88(2)–2.97(2); intrachain Ag···Ag 10.019(7); interchain, interstack Ag···Ag 8.410(8); N–Ag–N 178.5(9); N–Ag···O 83.4(5), 97.6(7); intrachain Ag···Ag···Ag 178.7(8).

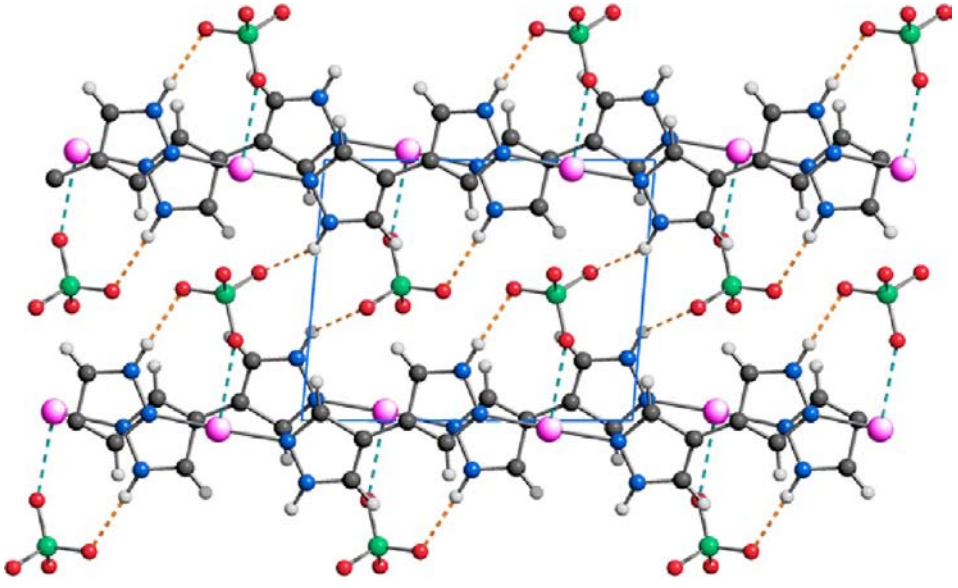

Figure 5. Representation of the crystal structure of species **3** viewed along *a*. Horizontal axis, *c*; vertical axis, *b*. Carbon, gray; hydrogen, light gray; chlorine, green; nitrogen, blue; oxygen, red; silver, fuchsia. Long Ag···O interactions and O···H–N hydrogen bonds are depicted with cyano and orange fragmented lines, respectively. Significant bond distances (Angstroms) and angles (degrees): Ag–N 2.16(2), 2.18(2); Ag···O 2.73(1); O···N–H 2.92(2), 3.07(3); intrachain Ag···Ag 10.014(5); interchain, interstack Ag···Ag 7.797(3); N–Ag–N 175.2(5); N–Ag···O 87.4(5), 92.9(5); intrachain Ag···Ag···Ag 180.

most of which are of more limited strength, involving not only the counterions and the N–H groups but also the clathrated water molecules, and overall contributing to the cohesiveness of the structure by bridging chains of adjacent stacks (Figure 4). In **3**, the perchlorate anions are involved in long Ag···O interactions, resulting into a AgN_2O T-shaped stereochemistry, and in weak hydrogen-bond interactions with adjacent N–H moieties (Figure 5).

Also in the case of **5**, the anions are involved with adjacent N–H groups in hydrogen bonds of limited strength. The overall cohesiveness at the supramolecular level is mainly granted by one of the two crystallographically independent counterions, which bridges chains of nearby columns by means of long Ag···F interactions (Figure 6). Each Ag(I) ion thus formally possesses a AgN_2F T-shaped stereochemistry.

dx.doi.org/10.1021/ic3011635 | *Inorg. Chem.* 2012, 51, 9775–9788

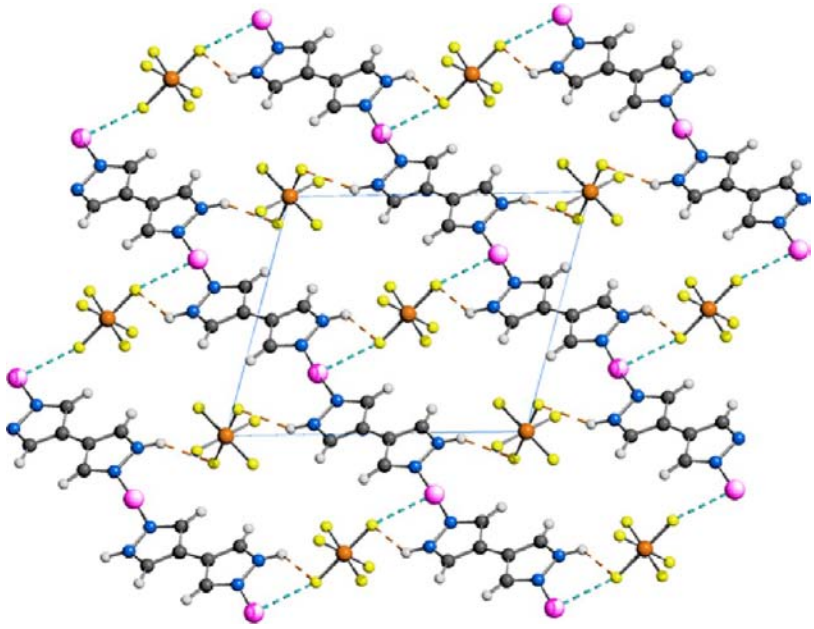

Figure 6. Representation of the crystal structure of species **5** viewed along *a*. Horizontal axis, *c*; vertical axis, *b*. Carbon, gray; hydrogen, light gray; nitrogen, blue; fluorine, yellow; phosphorus, orange; silver, fuchsia. Long Ag···F and F···H−N interactions are depicted with cyano and orange fragmented lines, respectively. Significant bond distances (Angstroms) and angles (degrees): Ag−N 2.11(1), 2.15(2); Ag···F 2.65(1), F···N−H 3.01(2)−3.16(3); intrachain Ag···Ag 10.02(1); interchain, interstack Ag···Ag 8.15(1); N−Ag−N 177(3); N−Ag···F 87(1), 93(1); intrachain Ag···Ag···Ag 178.0(1).

Even if preserving the 1-D structural motif in the same space group (Figure 7), dehydration of **2** promotes rearrangement of the overall crystal structure toward the non-isomorphous species **2a**, as witnessed by the halving of the unit cell volume (and, consequently, of the asymmetric unit). In **2a**, the metal centers are kept at about 10 Å, by *N*,*N*′-bridging H_2BPZ ligands, along chains running approximately along the [2 −3 0] direction and stacking along the [1 1 0] one. The counterions, disordered about a crystallographic inversion center, involve one of their oxygen atoms in a long Ag···O interaction and a second one in a hydrogen bond with the N−H residue of a chain belonging to the adjacent stack (Figure 7). On passing from **2** to **2a**, the absence of water molecules bridging chains belonging to neighbor columns implies a shortening of the interstack Ag···Ag distance from 8.410(8) to 7.2140(1) Å.

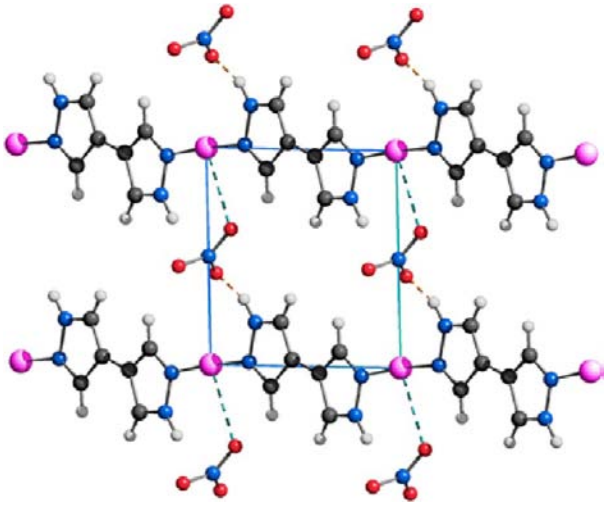

Figure 7. Representation of the crystal structure of species **2a** viewed along *a*. Horizontal axis, *b*; vertical axis, *c*. Carbon, gray; hydrogen, light gray; nitrogen, blue; oxygen, red; silver, fuchsia. Long Ag···O interactions and O···H−N hydrogen bonds are depicted with cyano and orange fragmented lines, respectively. For clarity, an ordered model in P1 has been adopted to draw the picture. Significant bond distances (Angstroms) and angles (degrees): Ag−N 2.129(3); Ag···O 2.97(6); O···N−H 2.64(8); intrachain Ag···Ag 10.058(6); interchain, interstack Ag···Ag 7.2141(4); N−Ag−N 180; N−Ag···O 72.2(9), 107.8(9); intrachain Ag···Ag···Ag 180.

Compound **4** crystallizes in the monoclinic space group *Pc*.[41] Its 1-D chains run approximately along the [−1 0 2] direction and pile up in columns along the [1 0 2] one (Figure 8). Along the chains, consecutive metal ions are kept ca. 10 Å apart by *N*,*N*′-*exo*-bidentate spacers; inter alia, being bisected by glide planes, the chains deviate from linearity (Ag···Ag···Ag ca. 163°), at variance with **2a**, **3**, **6**, and **7**, where linearity is imposed by symmetry, and with **2** and **5**, where only a slight deviation is observed (Ag···Ag···Ag ca. 178°). The counterions occupy the space among the columns and are involved in long Ag···F interactions as well as in weak F···H−N hydrogen bonds (Figure 8).

Compound **6** crystallizes in the orthorhombic space group *Pnna*. The [Ag(H_2BPZ)] chains run along the crystallographic axis *c*, with a bridged Ag···Ag distance equal to *c* and pile along *a* with a pace equal to *a*/2 (Figure 9). The counterions occupy the space among the piles of chains, lie almost parallel to the direction of piling, and are disordered about a crystallographic 2-fold axis. Each counterion is involved in a long Ag···O interaction and, with another oxygen atom, in a moderately weak hydrogen bond with an adjacent N−H moiety.

Finally, derivative **7** crystallizes in the monoclinic space group $P2_1$. Its 1-D chains run along the crystallographic axis *a*, with Ag···Ag bipyrazole-bridged distances equal to *a*, and stack along *b* at a distance of *b*/2. Each counterion completes the coordination sphere of one metal ion by means of a long Ag···O

dx.doi.org/10.1021/ic3011635 | *Inorg. Chem.* 2012, 51, 9775−9788

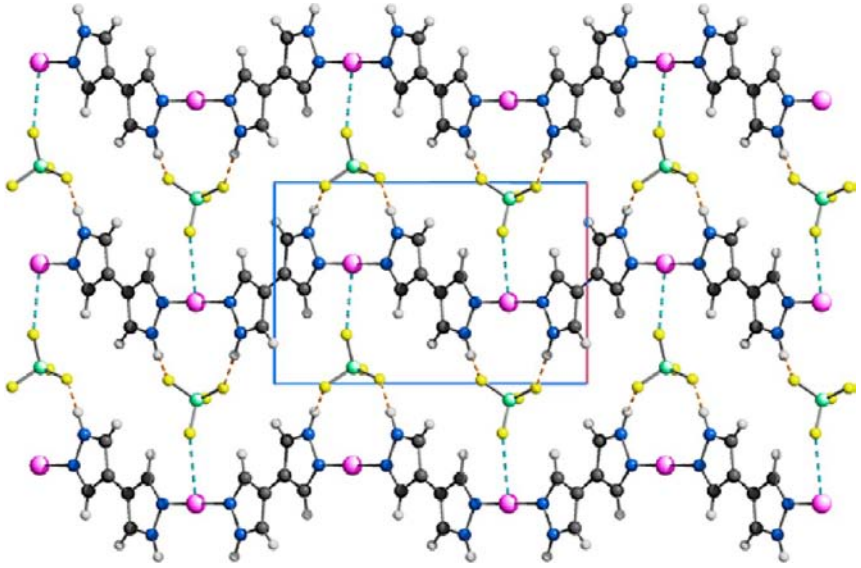

Figure 8. Representation of the crystal structure of species **4** viewed along *a*. Horizontal axis, *c*; vertical axis, *b*. Carbon, gray; hydrogen, light gray; boron, light green; fluorine, yellow; nitrogen, blue; silver, fuchsia. Long Ag···F and F···H−N interactions are depicted with cyano and orange fragmented lines, respectively. Significant bond distances (Angstroms) and angles (degrees): Ag−N 2.15(1), 2.17(1); Ag···F 2.76(2); F···N−H 2.71(4), 3.07(4); intrachain Ag···Ag 10.0195(6); interchain, interstack Ag···Ag 7.806(3); N−Ag−N 179(2); N−Ag···F 88 (1), 92(2); intrachain Ag···Ag···Ag 163.0(2).

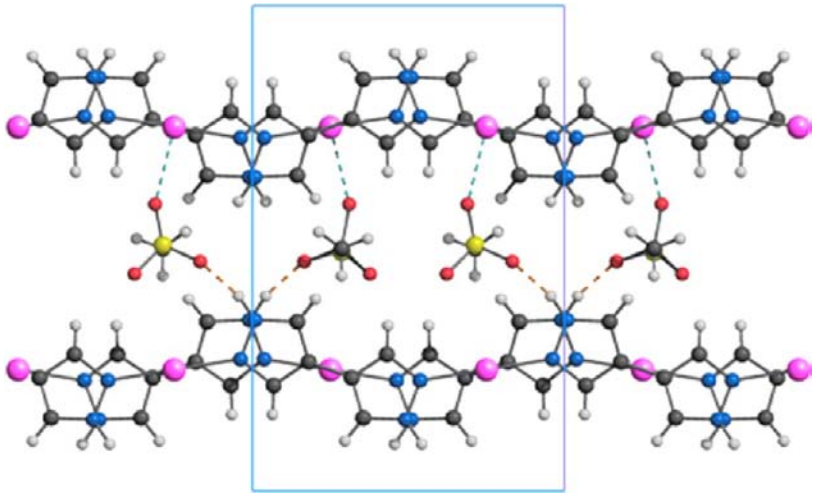

Figure 9. Representation of the crystal structure of species **6** viewed along *a*. Horizontal axis, *c*; vertical axis, *b*. Carbon, gray; hydrogen, light gray; nitrogen, blue; oxygen, red; sulfur, yellow; silver, fuchsia. Long Ag···O and O···H−N interactions are depicted with cyano and orange fragmented lines, respectively. Significant bond distances (Angstroms) and angles (degrees): Ag−N 2.161(6); Ag···O 2.63(2); O···N−H 2.62(2); intrachain Ag···Ag 10.0392(3); interchain, interstack Ag···Ag 7.8268(3); N−Ag−N 174(3); N−Ag···O 84.8(7), 93.9(8); intrachain Ag···Ag···Ag 180.

interaction and employs the other two oxygen atoms in hydrogen-bond interactions with N−H groups belonging to nearby stacks, thus augmenting the cohesiveness of the system along *c* (Figure 10).

Overall, the molecular and supramolecular characteristics of **2**, **3**, **6**, and **7** resemble those found in the analogous species $[Ag(Me_4BPZ)(NO_3)]\cdot CH_3OH$,[32] $[Ag(Me_4BPZ)(ClO_4)]$,[33] and $[Ag(Me_4BPZ)(CF_3SO_3)]$,[33] where linear, polycationic chains interact, at the metal centers, with nearby anions. In particular, in $[Ag(Me_4BPZ)(X)]$ (X = NO_3, ClO_4, CF_3SO_3), the interactions among the metal centers and counterions promote formation of double strands, as much as in **5**. None of the title materials show formation of helical strands, which are allowed, e.g., in $[Ag(Me_4BPZ)(PO_2F_2)]$ and $[Ag_4(Me_4BPZ)_5(NO_3)_4]$,[33] by the high deviation from planarity adopted by the Me_4BPZ ligand (higher than 60° in all cases). As for the title species, when allowed by symmetry (i.e., in **3**, **4**, **6**, and **7**), only a moderate deviation from planarity is observed, reaching the maximum value of ca. 9° in **7**.

3.4. Photoluminescence Properties. When exposed to UV irradiation at low temperature, many silver-based coordination polymers exhibit photoluminescence properties. Many may be the factors generating or tuning these functional properties, such as silver(I)−silver(I) interactions, enhancement of the intrinsic luminescence of the ligands due to cluster-based silver(I) centers, ligand-to-metal or metal-to-ligand charge transfers (LMCTs or MLCTs, respectively), and specific effects of the counterions.[2] Preliminary tests carried out with a UV lamp, in the solid state and at room temperature, revealed that **1**−**7** show photoluminescence emission but with different

dx.doi.org/10.1021/ic3011635 | *Inorg. Chem.* 2012, 51, 9775−9788

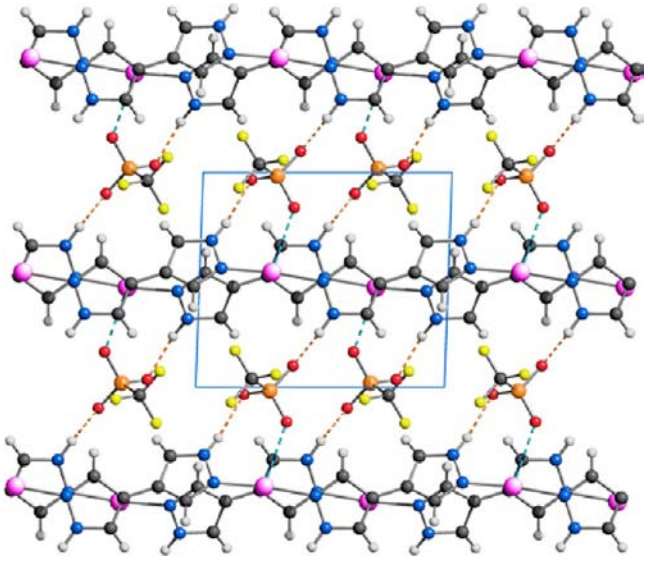

Figure 10. Representation of the crystal structure of species **7** viewed along *b*. Horizontal axis, *a*; vertical axis, *c*. Carbon, gray; hydrogen, light gray; nitrogen, blue; oxygen, red; sulfur, yellow; silver, fuchsia. Long Ag···O and O···H−N interactions are depicted with cyano and orange fragmented lines, respectively. Significant bond distances (Angstroms) and angles (degrees): Ag−N 2.12(2), 2.18(2); Ag···O 2.7(3); O···N−H 3.0 (2), 3.2(4); intrachain Ag···Ag 9.996(4); interchain, interstack Ag···Ag 8.635(5); N−Ag−N 159(1); N−Ag···O 80(6), 110(5); intrachain Ag···Ag···Ag 180.

intensity (Figure 11 left). Notably, the intensity of photoluminescence in the case of **4** and **6** is so weak that all attempts undertaken to acquire their emission spectra invariably failed. On the contrary, when excited at 330 nm, **1**−**3**, **5**, and **7** show a green-yellow photoluminescence emission (peaking in the narrow range 520−522 nm, Figure 11 right), suggesting their possible application as luminophores in the solid state and at room temperature. The low-energy emission bands observed can be reasonably ascribed to a MLCT excited state, in which the ligand LUMO orbitals are sufficiently low in energy to accept an excited electron from the electron-rich silver(I) center.[42] In the case of compound **1**, a contribution of the Ag···Ag interactions to the photoluminescence cannot be discarded.[1]

3.5. Microbiological Studies. The topical antibacterial activity of species **1**, **2**, and **4**−**7** was studied after their incorporation into PE disks. Two Gram-negative bacteria, *E. coli* and *P. aeruginosa*, and one Gram-positive bacterium, *S. aureus*, were selected as model. To substantiate the results, PE disks unloaded and loaded with $AgNO_3$ were tested as negative and positive controls, respectively. Prior to the tests, the PE disks were prepared and the bacterial cultures were grown as described in the Experimental Section.

To prove effective embedding, SEM images were acquired of both disk sides at different magnifications. In the case of the front side, contacted with the hot quartz surface during the embedding procedure, the acquired images (500×, 1500×, and 10 000×; Figure S8a−c, Supporting Information) revealed the presence of brighter zones which, according to X-ray fluorescence (XRF) spectroscopy measurements (Figure S9, Supporting Information), contain silver. When performed on the darker zones, XRF analyses did not reveal the presence of silver. Accordingly, the brighter zones can be confidently attributed to the embedded and homogeneously distributed silver(I) derivatives. The high roughness of the back side did not allow one to detect brighter zones, independently form the magnification applied (500× and 1500×; Figure S10a and S10b, Supporting Information).

To evaluate the amount of Ag(I) released, PE disks loaded with the coordination polymers and containing nearly the same amount of silver were suspended in distilled water under stirring; the content in Ag(I) of the suspending medium was monitored by ICP spectrometry at given time intervals. As expected for highly insoluble species, the concentration of silver(I) is on the ppm scale (**1** showing, inter alia, the lowest release), while an orders-of-magnitude higher release[43] is

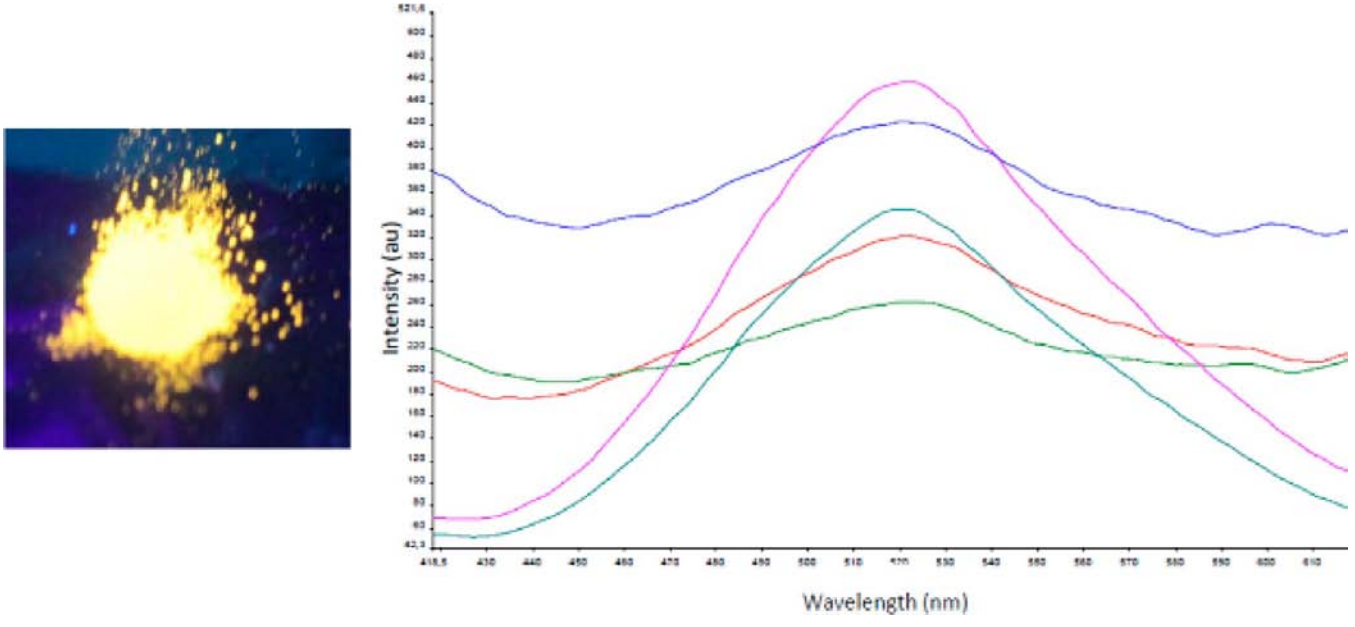

Figure 11. Photoluminescence emission of **2** under UV irradiation (left); emission spectra (right) of **1** (cyan), **2** (pink), **3** (red), **5** (green), and **7** (blue) after excitation at 330 nm.

dx.doi.org/10.1021/ic3011635 | *Inorg. Chem.* 2012, 51, 9775−9788

expected in the case of the strong electrolyte $AgNO_3$, this difference plausibly influencing the rate of antibacterial activity (see below). Worthy of note, after embedding into PE disks and left in contact with distilled water for 72 h, a slight darkening of the samples is observed, possibly due to formation of Ag(I)−hydr(oxo) species. In spite of this, all embedded polymers continue to express their biological activity also after 72 h.

In the following, the notations **DAg0**, **DAgNO$_3$**, and **DAg*N*** have been adopted to indicate PE disks unloaded, loaded with $AgNO_3$, and loaded with species ***N*** (*N* = **1**, **2**, and **4**−**7**), respectively.

Figure 12a shows the bacterial growth of three bacterial strains in the presence of a **DAg0**-type disk. As expected in the absence of an antibacterial agent, the bacterial charge increases with time, following the classic sigmoidal trend of the bacterial growth curves. The bactericidal effect of a **DAgNO$_3$**-type disk is depicted in Figures 12b and 12c in terms of CFU (colony forming unit) and percentage reduction, respectively: the bacterial charge is strongly diminished during the first 4 h of exposure, the reduction being above 90% after only 6 h and complete in 24 h, for all three bacteria tested (Figure 12c). A difference in the rate of action as a function of the bacterium can be appreciated: *S. aureus* is reduced of more than 90% already during the first 2 h.

Different performances, in terms of time and rate of action, resulted also from the tests carried out with **1**, **2**, and **4**−**7** (Figure 13; data shown in terms of CFU and percentage reduction). One hundred percent reduction of *E. coli* is achieved within 24 h of exposure by all **DAg*N***-type disks yet with a different rate than in the case of $AgNO_3$ (Figure 13e and 13f): while with **DAg1** the reduction reaches 90% in only 6 h, the other **DAg*N***-type disks show a slower activity. A similar behavior was observed against *P. aeruginosa* (Figure 13c and 13d): also in this case, all **DAg*N***-type disks attain complete reduction after 24 h of exposure. Again, **DAg1** shows the highest speed of action, allowing for a reduction of ca. 90% after 4 h. A markedly different behavior was appreciated against *S. aureus* (Figures 13a and 13b): similar to **DAgNO$_3$**, all **DAg*N***-type disks are strongly effective in the first period of exposure with a higher rate than against *E. coli* and *P. aeruginosa*. In fact, about 90% reduction is obtained in just 2 h. A significant slowing of the antibacterial activity follows this very fast initial reduction: complete reduction is obtained only after 24 h.

Notably, in the case of *P. aeruginosa* and *E. coli*, while complete reduction of the bacteria is achieved in 24 h both by $AgNO_3$ and by our coordination polymers, a lower rate of action is overall observed for the latter. As anticipated above, we cautiously attribute this diversity to the different amount of silver(I) released in the culture media by silver nitrate with respect to that freed by the coordination polymers. Worthy of note, lowering of the activity rate, rather than an annoying aspect, may be an advantageous feature. Indeed, soluble silver salts do not provide *prolonged* protection due to loss in concentration or complexation of the free Ag(I) ions. Thus, topical remedies containing silver in the form of soluble salts must be reapplied at frequent intervals. To slow the release of silver(I) ions during treatment, it has been recently proposed[44] to incorporate them in coordination polymers with varying degrees of solubility.

The performance of our coordination polymers does not appear, on the whole, remarkably different. As highlighted above, **DAg1** shows a higher initial rate of expression, which

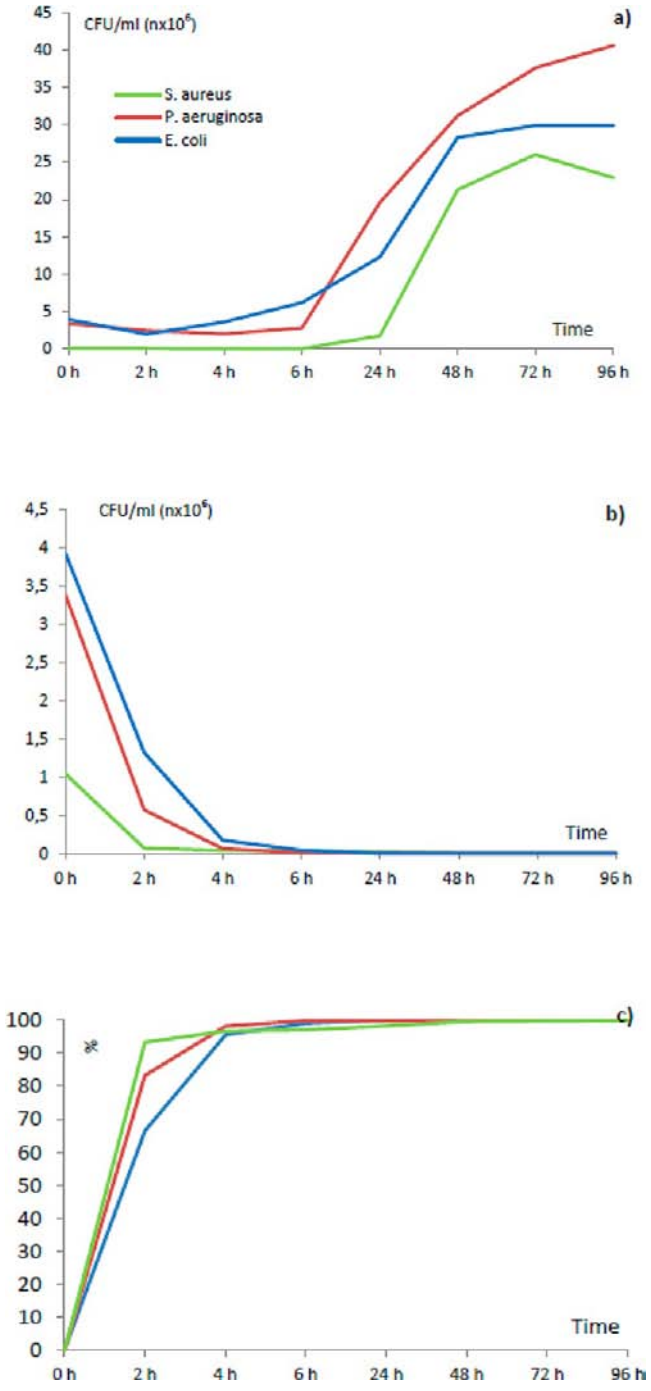

Figure 12. Antibacterial activity of control PE disks as a function of time: effect of a nonembedded PE disk, used as negative control, expressed in terms of CFU concentration (a). *E. coli* culture, blue; *P. aeruginosa* culture, red; *S. aureus* culture, light green. Effect of a PE disk embedded with $AgNO_3$, used as positive control, expressed in terms of CFU concentration (b) and percentage reduction (c).

may seem in contrast with its lowest silver(I) release. The lowest release by **DAg1** could be traced back to its 2-D network (vs the 1-D one of the other coordination polymers). Yet, its initial rate of action and, above all, the behavior of all coordination polymers suggest that there is no *neat* influence, on their *overall* antimicrobial activity, neither by the dimensionality of the coordination network, nor by the nature of the counterion, nor by the slight differences in terms of silver(I) release. We tentatively attribute this occurrence to the

dx.doi.org/10.1021/ic3011635 | *Inorg. Chem.* 2012, 51, 9775−9788

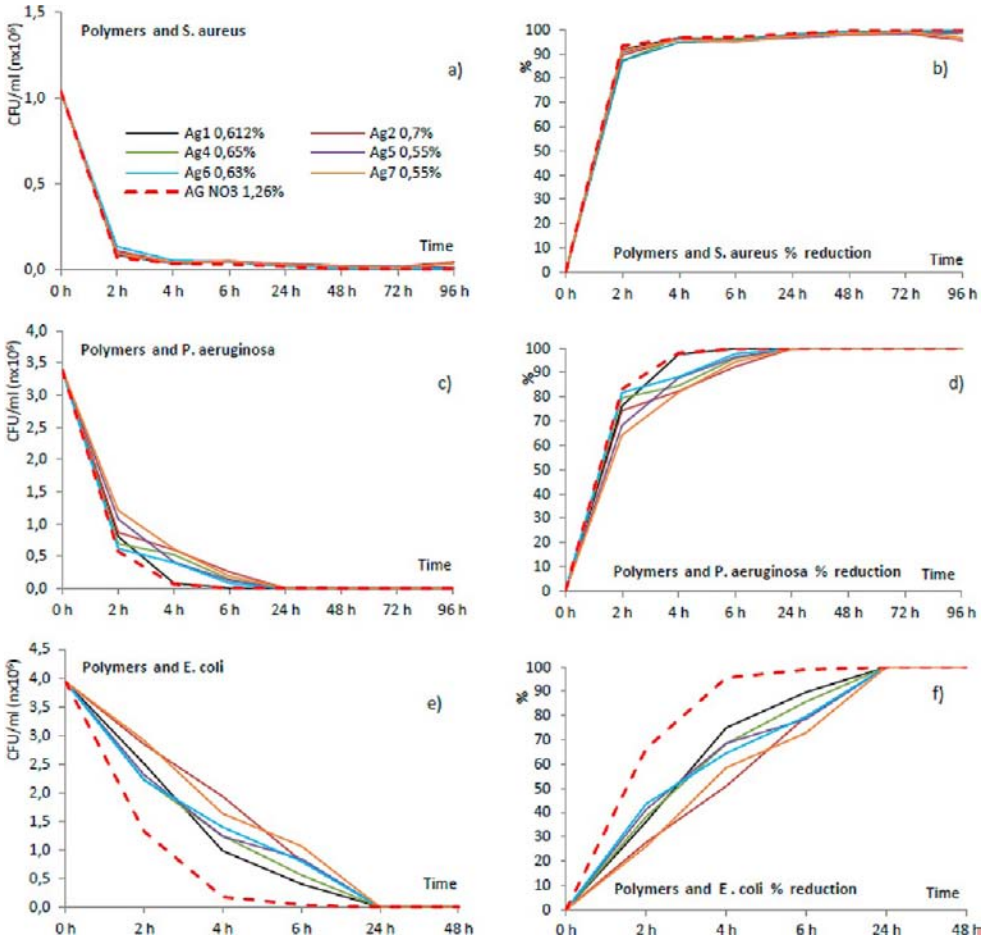

Figure 13. Antibacterial activity of PE disks embedded with species **1**, **2**, and **4**–**7** as a function of time, expressed in terms of CFU (left column) and percentage reduction (right column), against *S. aureus* (a and b), *P. aeruginosa* (c and d), and *E. coli* (e and f). For comparison, the activity of a PE disk embedded with $AgNO_3$ has been reported with a fragmented line. Colors adopted in the graphs as well as mass percentages of silver on the different disks are highlighted in the inset of a.

fact that all disks promote a saturation level of Ag(I) ions, as if the amount freed by these coordination polymers was, in all cases, higher than that needed for the antimicrobial activity to be expressed.

Finally, susceptibility tests were conducted to verify the biocidal activity by contact of the loaded PE disks. These tests clearly demonstrated inhibition of *E. coli* growth on the contact surface between the **DAg*N***-type disks and the bacterial lawn after a 24 h incubation of the m-FC Agar at 44 °C. As can be appreciated in Figure 14, the bacterial culture grows below **DAg0**, while no growth of bacteria is observed below **DAg4**.

As already recognized in the 1970s, when silver is used as a topical antimicrobial agent it is silver(I) ions which exert the biocidal effects.[45] Silver(I) ions bind to bacterial enzymes, thereby preventing them from performing their function, as well as to bacterial cell DNA, thus interfering with cell division and replication.[45] Silver(I) ions also interact with the negatively charged peptidoglycan present in the cell wall of the bacteria, impairing cell respiration (by blocking its energy transfer system) and eventually resulting in cell death.[46] Indeed, releasing their fluid and electrolyte content into the surrounding environment,[47] these cells dry, shrink, and die.[48]

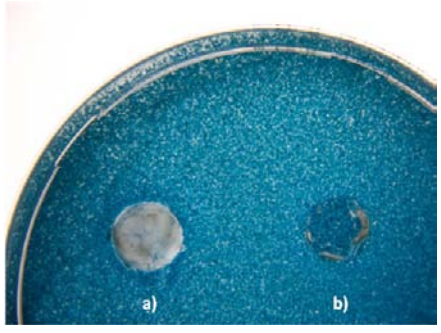

Figure 14. Bactericidal effect promoted by contact with a PE disk embedded with species **4** (a), compared to the effect of a non-embedded PE disk (b). Bacteria growth can be appreciated only below the non-embedded PE disk.

4. CONCLUSIONS

Reaction of the linear, ditopic ligand 4,4′-bipyrazole (H_2BPZ) with silver(I) salts allowed isolation and full characterization of the coordination polymers $[Ag_2(BPZ)]$ (**1**) and $[Ag(H_2BPZ)(X)]$ (X = NO_3, **2**; ClO_4, **3**; BF_4, **4**; PF_6, **5**; CH_3SO_3, **6**; CF_3SO_3, **7**), combining, in the solid state, room-temperature photoluminescence in the green-yellow region to antibacterial activity. Remarkably, when embedded into an inert matrix, all tested materials demonstrated to possess good bactericidal

dx.doi.org/10.1021/ic3011635 | *Inorg. Chem.* 2012, 51, 9775–9788

action against suspensions of model bacterial strains: 100% reduction is achieved against *E. coli*, *P. aeruginosa*, and *S. aureus* by all Ag(I) derivatives within 24 h. In the case of *S. aureus*, a reduction of about 90% is obtained in only 2 h. The bactericidal activity is expressed also by contact, as witnessed by contact susceptibility tests. No *neat* influence, on their *overall* antimicrobial activity, can be apparently attributed to the dimensionality of the coordination network, the nature of the counterion, or the slight differences in terms of silver(I) release. Remarkably, all show a lowering of the activity rate with respect to $AgNO_3$, which may be an advantageous feature in that they may provide *prolonged protection* and overcome the necessity of reapplying soluble silver salts at frequent intervals. These interesting results may be prodrome of further investigations, out of the scope of the present contribution, aiming to verify possible topical applications of the title silver(I)-based coordination polymers.

■ ASSOCIATED CONTENT

Ⓢ Supporting Information

Rietveld refinement plots for species **1**−**7** and **2a**, infrared spectra and TGA traces for species **1**−**7**, SEM images of both sides of the embedded PE disks, and X-ray fluorescence spectrum of the material embedded in the PE disks. This material is available free of charge via the Internet at http://pubs.acs.org.

■ AUTHOR INFORMATION

Corresponding Author

*E-mail: claudio.pettinari@unicam.it (C.P.); simona.galli@uninsubria.it (S.G.).

Notes

The authors declare no competing financial interest.

■ ACKNOWLEDGMENTS

Funding from the Universities of Camerino and Insubria is acknowledged. We are grateful to Ms. Anna Aulisio and Ms. Chiara Ortelli (University of Insubria) for their help in structural analysis and to Dr. Laura Petetta (University of Camerino) for her support in the acquisition of the SEM images.

■ REFERENCES

(1) See, e.g.: (a) Mak, T. C. W.; Zhao, X.-L. *Silver: Inorganic & Coordination Chemistry. Encyclopedia of Inorganic and Bioinorganic Chemistry*; John Wiley & Sons, Inc.: New York, 2011. (b) In *Design and Construction of Coordination Polymers*; Hong, M.-C., Chen, L., Eds.; John Wiley & Sons, Inc.: Hoboken, NJ, 2009; Chapters 1 and 5. (c) Chen, C.-L.; Kang, B.-S.; Su, C.-Y. *Aust. J. Chem.* **2006**, *59*, 3−18. (d) Khlobystov, A. N.; Blake, A. J.; Champness, N. R.; Lemenovskii, D. A.; Majouga, A. G.; Zyk, N. V.; Schröder, M. *Coord. Chem. Rev.* **2001**, *222*, 155−192.

(2) See, e.g.: (a) Farnum, G. A.; Knapp, W. R.; LaDuca, R. L. *Polyhedron* **2009**, *28*, 291−299. (b) Genuis, E. D.; Kelly, J. A.; Patel, M.; McDonald, R.; Ferguson, M. J. *Inorg. Chem.* **2008**, *47*, 6184−6194. (c) Luo, G.-G.; Huang, R.-B.; Chen, J.-H.; Lin, L.-R.; Zheng, L.-S. *Polyhedron* **2008**, *27*, 2791−2798. (d) Liu, S. Q.; Kuroda-Sowa, T.; Konaka, H.; Suenaga, Y.; Maekawa, M.; Mizutani, T.; Ning, G. L.; Munakata, M. *Inorg. Chem.* **2005**, *44*, 1031−1036.

(3) See, e.g.: (a) Bloch, W. M; Sumby, C. J. *Chem. Commun.* **2012**, 2534−2536. (b) May, L. J.; Shimizu, G. K. H. *Chem. Mater.* **2005**, *17*, 217−220. (c) Yang, G.; Raptis, R. G. *Chem. Commun.* **2004**, 2058−2059. (d) Mäkinen, S. K.; Melcer, N. J.; Parvez, M.; Shimizu, G. K. H. *Chem.—Eur. J.* **2001**, *7*, 5176−5182.

(4) See, e.g.: (a) Zhang, J.-P.; Kitagawa, S. *J. Am. Chem. Soc.* **2008**, *130*, 907−917. (b) Zhang, J.-P.; Horike, S.; Kitagawa, S. *Angew. Chem., Int. Ed.* **2007**, *46*, 889−892. (c) Xu, X.; Nieuwenhuyzen, M.; James, S. L. *Angew. Chem., Int. Ed.* **2002**, *41*, 764−767.

(5) See, e.g.: (a) Zheng, X.-F.; Zhu, L.-G. *CrystEngComm* **2010**, *12*, 2878−2884. (b) Lin, P.; Henderson, R. A.; Harrington, R. W.; Clegg, W.; Wu, C.-D.; Wu, X.-T. *Inorg. Chem.* **2004**, *43*, 181−188. (c) Fu, R.; Xia, S.; Xiang, S.; Hu, S.; Wu, X. *J. Solid State Chem.* **2004**, *177*, 4626−4631.

(6) See, e.g.: (a) Wang, R. H.; Xu, L. J.; Li, X. S.; Li, Y. M.; Shi, Q.; Zhou, Z. Y.; Hong, M. C.; Chan, A. S. C. *Eur. J. Inorg. Chem.* **2004**, 1595−1599. (b) Caradoc-Davies, P. L.; Hanton, L. R. *Chem. Commun.* **2001**, 1098−1099. (c) Konno, T.; Yoshimura, T.; Aoki, K.; Okamoto, K.-I.; Hirotsu, M. *Angew. Chem., Int. Ed.* **2001**, *40*, 1765−1768.

(7) See, e.g.: (a) Yamada, S.; Ishida, T.; Nogami, T. *Dalton Trans.* **2004**, 898−903. (b) Zhang, D. Q.; Ding, L.; Xu, W.; Hu, H. M.; Zhu, D. B.; Huang, Y. H.; Fang, D. C. *Chem. Commun.* **2002**, 44−45.

(8) See, e.g.: (a) Berchel, M.; Le Gall, T.; Denis, C.; Le Hir, S.; Quentel, F.; Elléouet, C.; Montier, T.; Rueff, J.-M.; Salaün, J.-Y.; Haelters, J.-P.; Hix, G. B.; Lehn, P.; Jaffrès, P.-A. *New J. Chem.* **2011**, *35*, 1000−1003. (b) Brunetto, P. S.; Slenters, T. V.; Fromm, K. M. *Materials* **2011**, *4*, 355−367. (c) Slenters, T. V.; Hauser-Gerspach, I.; Daniels, A. U.; Fromm, K. M. *J. Mater. Chem.* **2008**, *18*, 5359−5362.

(9) (a) Mohamed, A. A. *Coord. Chem. Rev.* **2010**, *254*, 1918−1947.

(10) See, e.g.: (a) Patra, G. K.; Goldberg, I.; De, S.; Datta, D. *CrystEngComm* **2007**, *9*, 828−832. (b) Feazell, R. P.; Carson, C. R.; Klausmeyer, K. K. *Inorg. Chem.* **2006**, *45*, 2627−2634. (c) Feazell, R. P.; Carson, C. R.; Klausmeyer, K. K. *Inorg. Chem.* **2006**, *45*, 2635−2643. (d) Burchell, T. J.; Eisler, D. J.; Puddephatt, R. J. *Cryst. Growth Des.* **2006**, *6*, 974−982. (e) Seward, C.; Chan, J.; Song, D.; Wang, S. *Inorg. Chem.* **2003**, *42*, 1112−1120.

(11) Blake, A. J.; Champness, N. R.; Cooke, P. A.; Nicolson, J. E. B. *Chem. Commun.* **2000**, 665−666.

(12) Pettinari, C.; Masciocchi, N.; Pandolfo, L.; Pucci, D. *Chem.—Eur. J.* **2010**, *16*, 1106−1123.

(13) Rawashdeh-Omary, M. A.; Rashdan, M. D.; Dharanipathi, S.; Elbjeirami, O.; Ramesh, P.; Rasika Dias, H. V. *Chem. Commun.* **2011**, *47*, 1160−1162.

(14) Tsukuda, T.; Kawase, M.; Dairiki, A.; Matsumoto, K.; Tsubomura, T. *Chem. Commun.* **2010**, *46*, 1905−1907.

(15) See, e.g.: Zhao, G.; Stevens, S. E., Jr. *Biometals* **1998**, *11*, 27−32.

(16) Fox, C. L. *AMA Arch. Surg.* **1968**, *96*, 184−188.

(17) Catauro, M.; Raucci, M. G.; De Gaetano, F. D.; Marotta, A. *J. Mater. Sci. Mater. Med.* **2004**, *15*, 831−837.

(18) Crabtree, J. H.; Burchette, R. J.; Siddiqi, R. A.; Huen, I. T.; Handott, L. L.; Fishman, A. *Peritoneal Dial. Int.* **2003**, *23*, 368−374.

(19) See, e.g.: (a) Chen, W.; Liu, Y.; Courtney, H. S.; Bettenga, M.; Agrawal, C. M.; Bumgardner, J. D. *Biomaterials* **2006**, *27*, 5512−5517. (b) Bosetti, M.; Massè, A.; Tobin, E.; Cannas, M. *Biomaterials* **2002**, *23*, 887−892. (c) Kramer, S. J.; Spadaro, J. A.; Webster, D. A. *Clin. Orthop. Relat. Res.* **1981**, *161*, 154−162.

(20) See, e.g.: Durán, N.; Marcato, P. D.; De Souza, G. I. H.; Alves, O. L.; Esposito, E. *J. Biomed. Nanotech.* **2007**, *3*, 203−208.

(21) (a) Nomyia, K.; Tsuda, K.; Sudoh, T.; Oda, M. *J. Inorg. Biochem.* **1997**, *68*, 39−44. (b) Nomiya, K.; Tsuda, K.; Tanabe, Y.; Nagano, H. *J. Inorg. Biochem.* **1998**, *69*, 9−14. (c) Nomiya, K.; Tsuda, K.; Kasuga, N. C. *J. Chem. Soc., Dalton Trans.* **1998**, 1653−1659. (d) Nomiya, K.; Noguchi, R.; Oda, M. Unpublished results. (e) Nomiya, K.; Noguchi, R.; Oda, M. *Inorg. Chim. Acta* **2000**, *298*, 24−32. (f) Nomiya, K.; Onoue, K.; Kondoh, Y.; Kasuga, N. C.; Nagano, H.; Oda, M.; Sakuma, S. *Polyhedron* **1995**, *14*, 1359−1367. (g) Nomiya, K.; Kondoh, Y.; Onoue, K.; Kasuga, N. C.; Nagano, H.; Oda, M.; Sudoh, T.; Sakuma, S. *J. Inorg. Biochem.* **1995**, *58*, 255−267. (h) Nomiya, K.; Noguchi, R.; Kato, C. *Chem. Lett.* **2000**, 162−163.

(22) Kasuga, N. C.; Yoshikawa, R.; Sakai, Y.; Nomiya, K. *Inorg. Chem.* **2012**, *51*, 1640−1647.

(23) Boldog, I.; Sieler, J.; Chernega, A. N.; Domasevitch, K. V. *Inorg. Chim. Acta* **2002**, *338*, 69−77.

(24) Lozan, V.; Solntsev, P. Y.; Leibeling, G.; Domasevitch, K. V.; Kersting, B. *Eur. J. Inorg. Chem.* **2007**, 3217−3226.
(25) Sun, Q.-F.; Wong, K. M.-C.; Liu, L.-X.; Huang, H.-P.; Yu, S.-Y.; Yam, V. W.-W.; Li, Y.-Z.; Pan, Y.-J.; Yu, K.-C. *Inorg. Chem.* **2008**, *47*, 2142−2154.
(26) (a) Masciocchi, N.; Galli, S.; Sironi, A. In *Techniques in Inorganic Chermistry*; Fackler, J. P., Falvello, L., Eds.; CRC Press Taylor and Francis: Boca Raton, FL, 2010. (b) Masciocchi, N.; Galli, S.; Colombo, V.; Maspero, A.; Palmisano, G.; Seyyedi, B.; Lamberti, C.; Bordiga, S. *J. Am. Chem. Soc.* **2010**, *132*, 7902−7904. (c) Galli, S.; Masciocchi, N.; Colombo, V.; Maspero, A.; Palmisano, G.; López-Garzón, F. J.; Domingo-García, M.; Fernández-Morales, I.; Barea, E.; Navarro, J. A. R. *Chem. Mater.* **2010**, *22*, 1664−1672. (d) Colombo, V.; Galli, S.; Choi, H. J.; Han, G. D.; Maspero, A.; Palmisano, G.; Masciocchi, N.; Long, J. R. *Chem. Sci.* **2011**, *2*, 1311−1319.
(27) Pettinari, C.; Tabacaru, A.; Boldog, I.; Domasevitch, K. V.; Galli, S.; Masciocchi, N. *Inorg. Chem.* **2012**, *51*, 5235−5245.
(28) Coelho, A. *J. Appl. Crystallogr.* **2003**, *36*, 86−95.
(29) *TOPAS*, Version 3.0; Bruker AXS: Karlsruhe, Germany 2005.
(30) To describe the ligand, the *z*-matrix formalism was used, imposing idealized bond distances and angles, as follows: C−C, C−N, and N−N of the heterocyclic ring 1.36 Å; C−C of the arene 1.39 Å; exocyclic C−C 1.50 Å; C−H, N−H = 0.95 Å; heterocyclic ring internal bond angles 108°; arene internal and external bond angles 120°.
(31) Buchner, E. *Berichte* **1889**, *22*, 842.
(32) Boldog, I.; Rusanov, E. B.; Chernega, A. N.; Sieler, J.; Domasevitch, K. V. *Polyhedron* **2001**, *20*, 887−897.
(33) Domasevitch, K. V.; Boldog, I.; Rusanov, E. B.; Hunger, J.; Blaurock, S.; Schöder, M.; Sieler, J. *Z. Anorg. Allg. Chem.* **2005**, *631*, 1095−1100.
(34) Lever, A. B. P.; Mantovani, E.; Ramaswamy, B. S. *Can. J. Chem.* **1971**, *49*, 1957−1964.
(35) Rosenthal, M. R. *J. Chem. Educ.* **1973**, *50*, 331−334.
(36) (a) Miles, M. G.; Doyle, G.; Cooney, R. P.; Tobias, R. S. *Spectrochim. Acta A* **1969**, *25*, 1515−1526. (b) Panicker, C. Y.; Varghese, H. T.; Philip, D.; Nogueira, H. I. S. *Spectrochim. Acta A* **2006**, *64*, 744−747. (c) Bala, R.; Sharma, R. P.; Bond, A. D. *J. Mol. Struct.* **2007**, *830*, 198−203.
(37) Easy release of HCN from H_2BPZ, impossible from pz and Me_4BPZ, cannot be excluded.
(38) Yang, G.; Raptis, R. G. *Inorg. Chem.* **2003**, *42*, 261−263.
(39) (a) Rasika Dias, H. V.; Diyabalanage, H. V. K. *Polyhedron* **2006**, *25*, 1655−1661. (b) Kishimura, A.; Yamashita, T.; Aida, T. *J. Am. Chem. Soc.* **2005**, *127*, 179−183. (c) Rasika Dias, H. V.; Diyabalanage, H. V. K.; Eldabaja, M. G.; Elbjeirami, O.; Rawashdeh-Omary, M. A.; Omary, M. A. *J. Am. Chem. Soc.* **2005**, *127*, 7489−7501. (d) Omary, M. A.; Rawashdeh-Omary, M. A.; Gonser, M. W. A.; Elbjeirami, O.; Grimes, T.; Cundari, T. R. *Inorg. Chem.* **2005**, *44*, 8200−8210.
(40) Masciocchi, N.; Moret, M.; Cairati, P.; Sironi, A.; Ardizzoia, G. A.; La Monica, G. *J. Am. Chem. Soc.* **1994**, *116*, 7668−7676.
(41) Obviously, possessing *P*2/*c* the same systematic absences as *Pc*, an alternative description in *P*2/*c*, implying a disordered BF_4 anion, cannot be excluded but was here discarded in favor of the simpler model in *Pc*.
(42) Zhang, J.-P.; Lin, Y. Y.; Huang, X. C.; Chen, X. M. *J. Am. Chem. Soc.* **2005**, *127*, 5495−5506.
(43) From the point of view of thermodynamics. Indeed, $AgNO_3$ solubility in water at 20 °C is 2160 g/L, i.e., 12 M.
(44) (a) Vermeulen, H.; van Hattem, J. M.; Storm-Versloot, M. N.; Ubbink, D. T.; Westerbos, S. J. *Cochrane Database of Systematic Reviews*; 2007; Vol. *1*, p CD005486 and references therein. (b) Rogers, R. S. *13th Annual Symposium on Advanced Wound Care*, Dallas, TX, 2000.
(45) Thompson, S. In *Comprehensive Inorganic Chemistry*; Bailey, J. C., Ed.; Pergamon Press: Oxford, UK, 1973; pp 79−128.
(46) (a) Lansdown, A. B. *J. Wound Care* **2002**, *11*, 125−30. (b) Nawaz, M.; Han, M. Y.; Kim, T.; Manzoor, U.; Amin, M. T. *Sci. Total Environ.* **2012**, *431*, 20−25.
(47) Jung, W. K.; Koo, H. C.; Kim, K. W.; Shin, S.; Kim, S. H.; Park, Y. H. *Appl. Environ. Microbiol.* **2008**, *74*, 2171−2178.
(48) Guggenbichler, J.-P.; Böswald, M.; Lugauer, S.; Krall, T. *Infection* **1999**, *27*, 16−22.